Electronic Supplementary Information (ESI†)

Multihalogenated Zn phthalocyanine as a precursor for porous Zn–N_4–C carbons toward electrocatalytic oxygen reduction

Keisuke Sakamoto, Yasuhiro Shiraishi,* Keisuke Kinoshita, Koki Yoshida,
Wataru Hiramatsu, and Takayuki Hirai

shiraishi.yasuhiro.es@osaka-u.ac.jp

CONTENTS

Methods

General

Water was purified by the Milli-Q system. ZnPc and G58 were supplied from DIC Corp. A 5 wt% Nafion dispersion (DE521CS) and other chemicals were purchased from Wako. The Pt/C catalyst (Pt 10 wt%, TEC10E10E) was purchased from Tanaka Precious Metals. All reagents were used without further purification.

Synthesis of catalysts

The catalysts were prepared by pyrolysis of ZnPc or G58 under N_2 gas flow (50 mL min^{-1}) or 10% NH_3/He mixed gas flow (50 mL min^{-1}) in a tubular furnace at 1173 K, with a heating rate of 10 K min^{-1} and a holding time of 2 h, respectively.

LSV measurements

The LSV measurements were performed at room temperature in a RRDE system (RRDE-3A, BAS) using 0.1 M KOH (pH 13.0, 65 mL) as an electrolyte. The Pt coil and Ag/AgCl electrodes were used as the counter and reference electrodes, respectively. The working RRDE electrode was prepared as follows: the catalyst ink was made by ultrasonication of a mixture of pure water (1680 μL), catalyst (12.3 mg), 5 wt% Nafion dispersion (30 μL), and 2-propanol (420 μL). The ink (10 μL) was put onto a surface-polished glassy carbon electrode (4 mm diameter, 0.1257 cm^2) and dried at room temperature, where the mass density of the catalyst was 0.46 mg cm^{-2}. All potential values were referred to the reversible hydrogen electrode (RHE) using the following equation.[1]

$$E(vs\ \mathrm{RHE}) = E(vs\ \mathrm{Ag/AgCl}) + 0.197 + 0.059 \times \mathrm{pH}$$

Prior to measurements, N_2 gas was bubbled through the electrolyte for 30 min, and cyclic voltammetry (CV) cycles (0.3–1.0 V (vs RHE)) were performed for 200 cycles for cleaning and activation of the catalyst. Then, O_2 was bubbled through the electrolyte for 30 min, and LSV measurements were performed at between 1.0 V to 0.3 V (vs RHE) with a scan rate of 2 mV s^{-1} and a rotation speed of 1600 rpm. To exclude the capacitive effects, the obtained LSV curves were normalized by subtracting the data obtained in N_2-saturated electrolyte.[2] During the measurements, the ring electrode potential was maintained at 1.1 V (vs RHE). The electron transfer number (n) per O_2 during ORR on the electrode was determined using the following equation:

$$n = \frac{4 \times I_\mathrm{D}}{I_\mathrm{D} + {I_\mathrm{R}}/{N}}$$

I_D is the disk current, I_R is the ring current, and N is the collection efficiency of the ring ($N = 0.424$),[3] respectively.

Analysis

SEM observations were performed using a JSM-7800F microscope (JEOL). XPS spectra were obtained on a PHI GENESIS spectrometer (ULVAC-PHI) with a monochromatic Al Kα radiation

(1486.6 eV), where the obtained spectra were calibrated with respect to the sp2 carbon peak (284.6 eV). The MultiPak software (ULVAC-PHI) was used for the deconvolution of the spectra using Gauss-Lorentz equations with a Shirley-type background, where the 70 % Gaussian/30 % Lorentzian line shape was used to evaluate the peak positions and areas.[4] The N_2 adsorption/desorption measurements were performed at 77 K using a BELSORP MAX X (Microtrac BEL). The specific surface areas were determined on the basis of the Brunauer–Emmett–Teller (BET) method, and the pore size distributions were determined based on the Barrett–Joyner–Halenda (BJH)[5] and micropore (MP) methods,[6] respectively. The TG-DTA/EI-MS analysis was performed on a Thermo Mass Photo system (Rigaku) using He as a carrier gas. The powder XRD patterns were recorded on the SmartLab (Rigaku) X-ray diffractometer with a Cu-Kα radiation. The STEM images were acquired using a JEM-ARM300F (JEOL) microscope at an accelerating voltage of 80 kV, and STEM-EDS observations were conducted on a JEM-ARM300F (JEOL) microscope at 80 kV. The Zn contents of the samples were determined by using an inductively coupled plasma-optical emission spectrometry (ICP-OES, Agilent 5800), after dissolving the samples in nitric acid under microwave irradiation. Raman spectra were recorded on an NRS-5500 instrument (JASCO) with a 532 nm excitation laser.

Table S1 Elemental compositions (wt%) of the respective samples.

	C[a]	N[a]	H[a]	Br[a]	Cl[a]	Zn[b]
ZnPc[c]	66.5	19.4	2.8			11.3
G58[d]	20.9–66.5	6.1–19.4	<2.8	<69.5	<50.2	3.6–11.3
ZnPc_N_2	76.4	11.6	<0.1[e]			11.0
ZnPc_NH_3	73.2	13.0	0.1[e]			11.0
G58_N_2	73.7	9.6	1.0[e]	0.2	<0.1	1.7
G58_NH_3	68.5	11.6	1.2[e]	0.4	<0.1	5.2

[a] Determined by the combustion method.

[b] Determined by the ICP–OES analysis.

[c] The theoretical values determined from the ZnPc structure.

[d] The theoretical values calculated from ZnPc, ZnPc-Cl_{16}, and ZnPc-Br_{16} structures.

[e] The H component may be attributable to the adsorbed water.

Table S2 The ORR performance and preparation procedures of the reported Zn–N_4–C catalysts.[a]

Sample name	Reagents used for catalyst preparation	Procedure	Onset potential / V vs RHE [b]	Half-wave potential / V vs RHE [c]	Current density @0.4 V, @1600 rpm / mA cm^{-2}	Ref
Zn-N-C	ZnPc, mesoporous silica (SBA-15)	pyrolysis (10 K min^{-1}), acid washing (5 wt% HF)	0.85	0.75	2.8 [d]	[7]
NC-0.5-S	$ZnCl_2$, 4,4′-bipyridine, SBA-15	pyrolysis (2 K min^{-1}), acid washing (40 wt% HF)	0.97	0.89	5.3	[8]
NDCF(Zn)-H2	ZnPc, NaCl	multiple pyrolysis, acid washing (0.5 M H_2SO_4)	1.01	0.88	5.9	[9]
Zn-N-C-1	$ZnCl_2$, $NH_4S_2O_8$, o-phenylenediamine	multiple pyrolysis (1 K min^{-1}), acid washing (1 M HCl)	0.96	0.87	5.0	[10]
Zn_1-2D-NOC	ZnPc, urea, dicyandiamide	pyrolysis (10 K min^{-1}), acid washing (37% HCl)	0.81	0.69	1.0	[11]
ZnN_x/BP	$Zn(OAC)_2{\cdot}2H_2O$, urea carbon black (BP2000)	pyrolysis, acid washing (6 M HNO_3)	1.06	0.85	6.0	[12]
G58_NH_3	G58 green pigment	pyrolysis (10 K min^{-1}) under 10% NH_3/He flow	0.91	0.78	5.4	This work

[a] The ORR performance in all systems was monitored in 0.1 M KOH.

[b] The potential that generates a current density of < –0.1 mA cm^{-2}.

[c] The potential that generates half the maximum current density.

[d] The data obtained at 900 rpm.

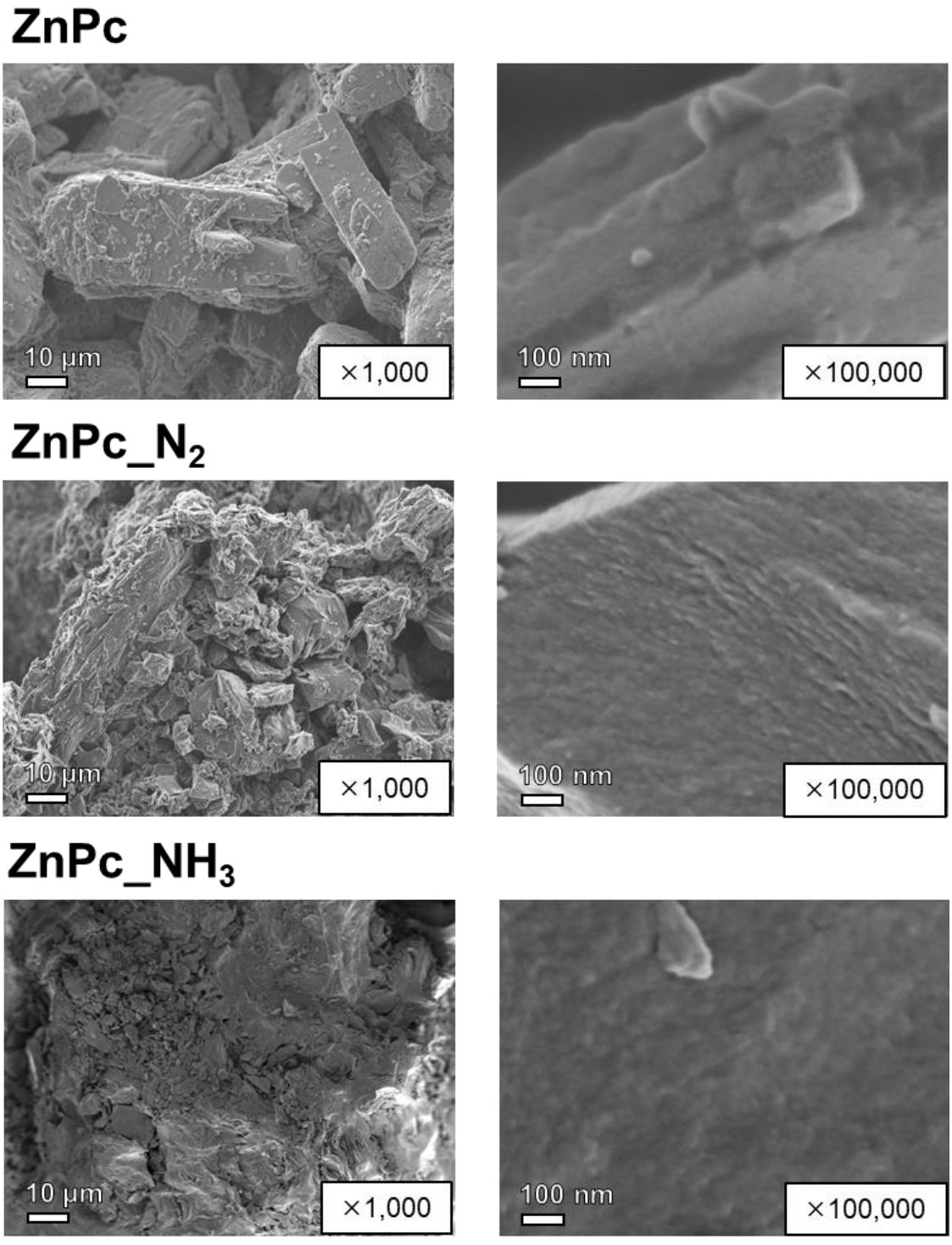

Fig. S1 SEM images of ZnPc, ZnPc_N_2, and ZnPc_NH_3.

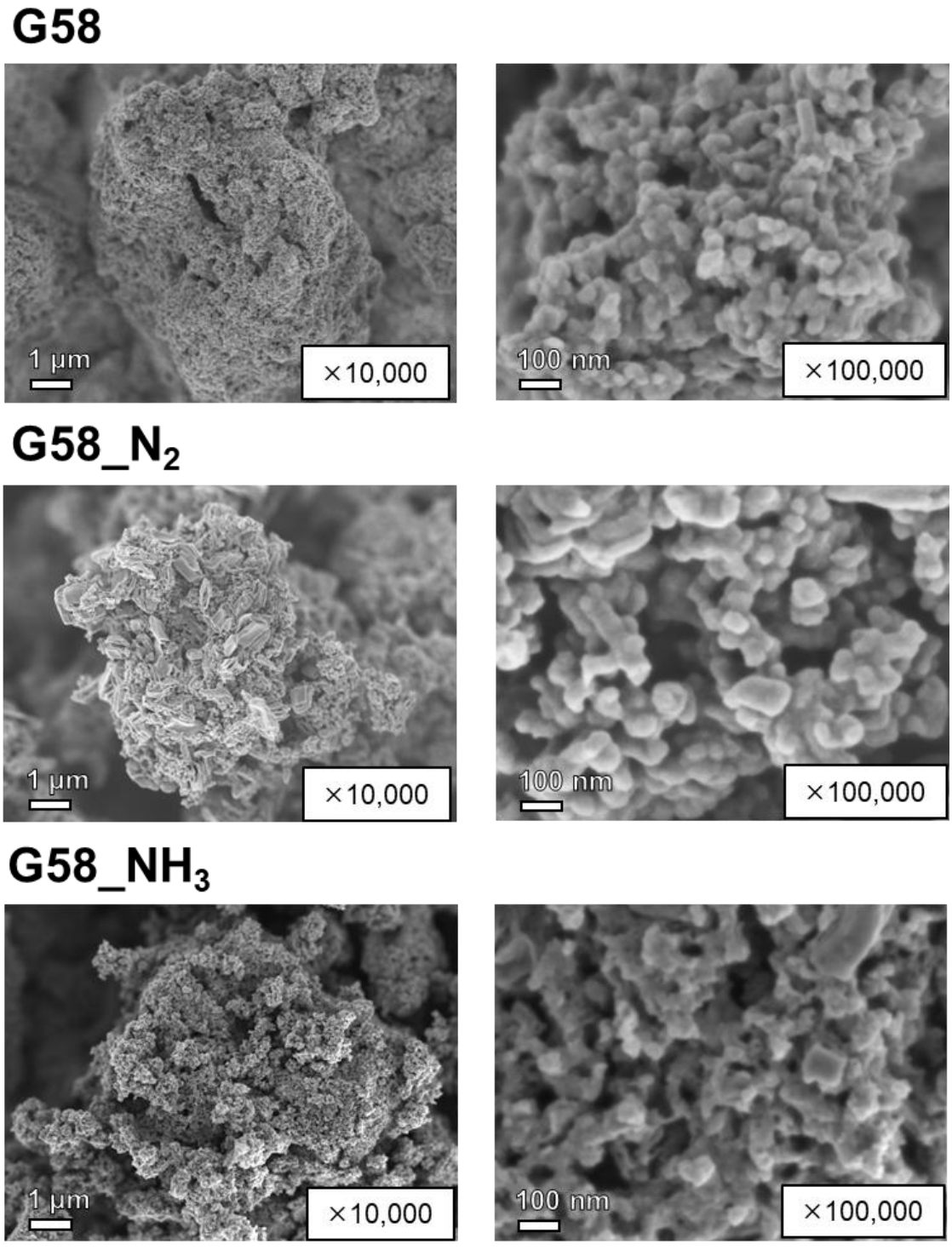

Fig. S2 SEM images of G58, G58_N_2, and G58_NH_3.

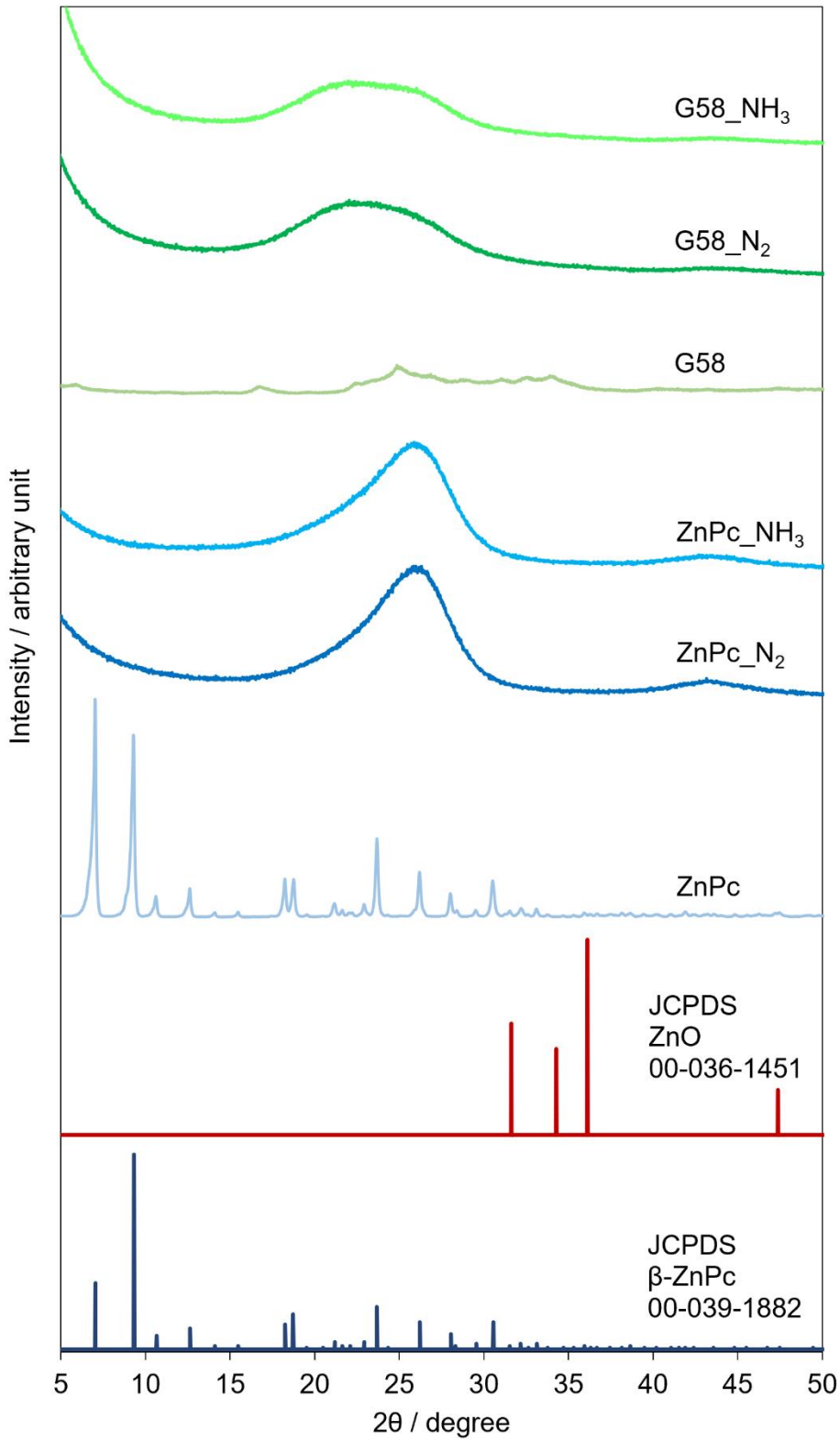

Fig. S3 Powder XRD patterns of ZnPc and G58 and their corresponding carbons.

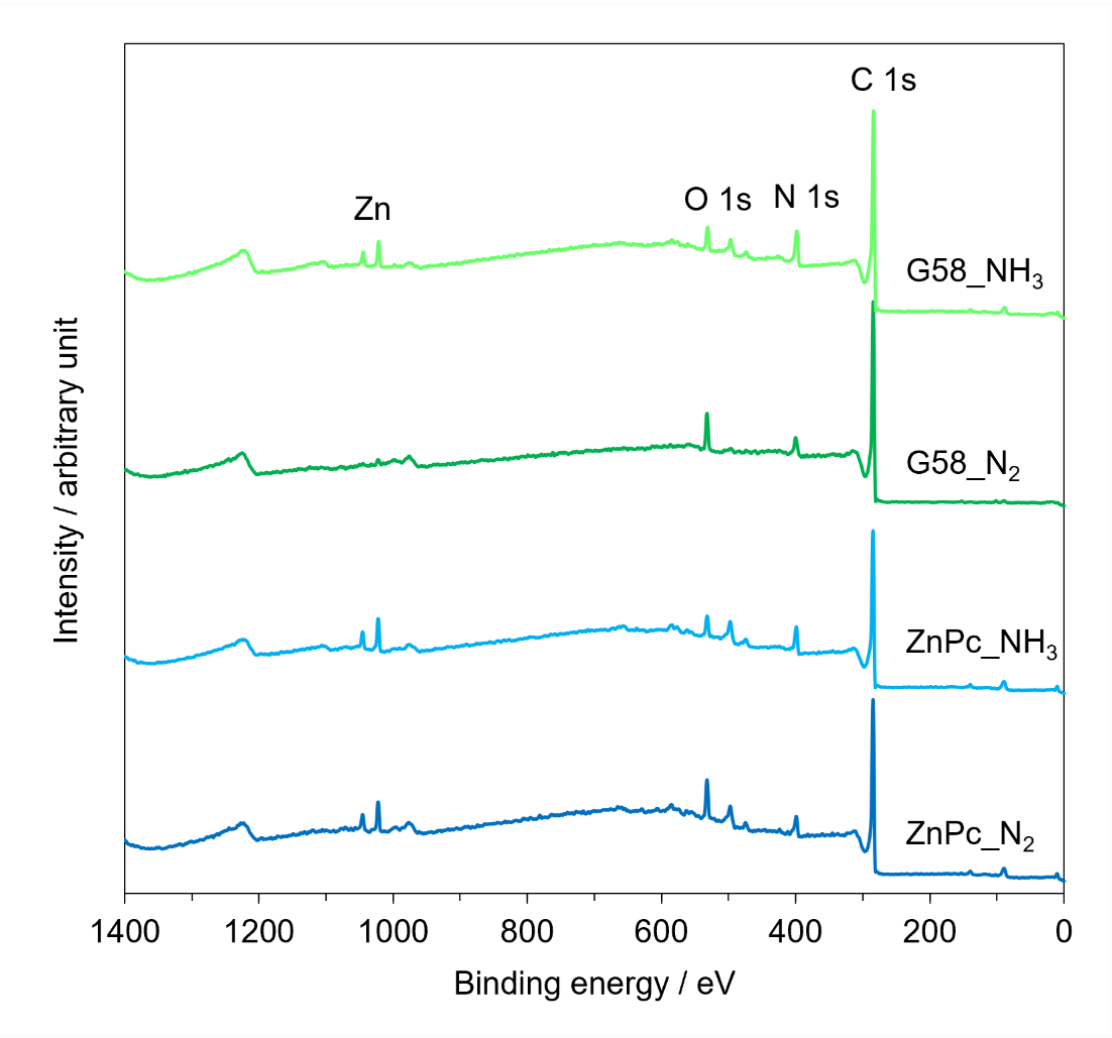

Fig. S4 The XPS survey spectra of the carbons.

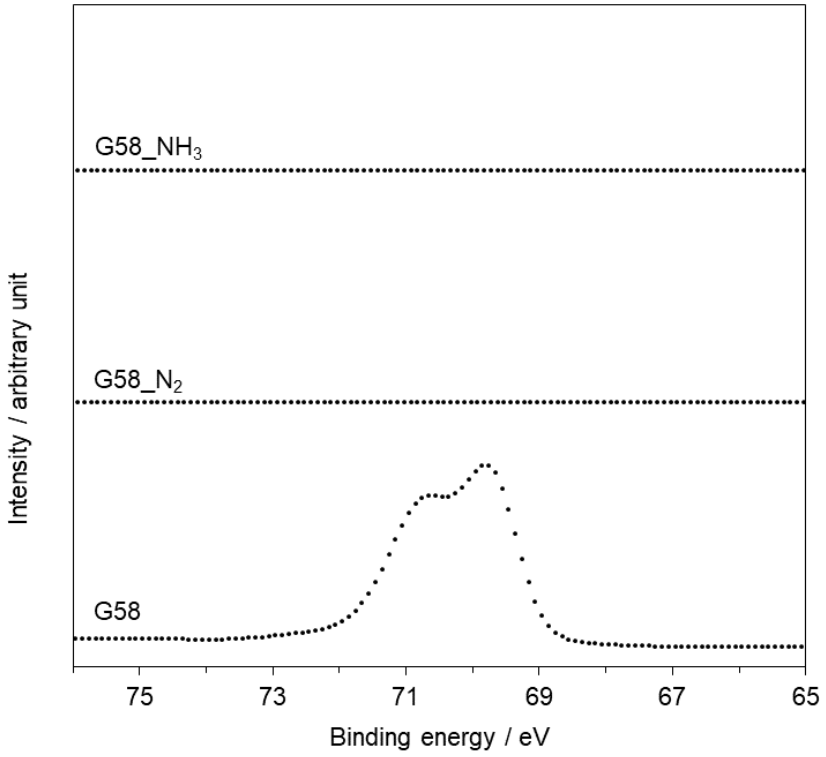

Fig. S5 The Br 3d XPS spectra of G58 and its corresponding carbons.

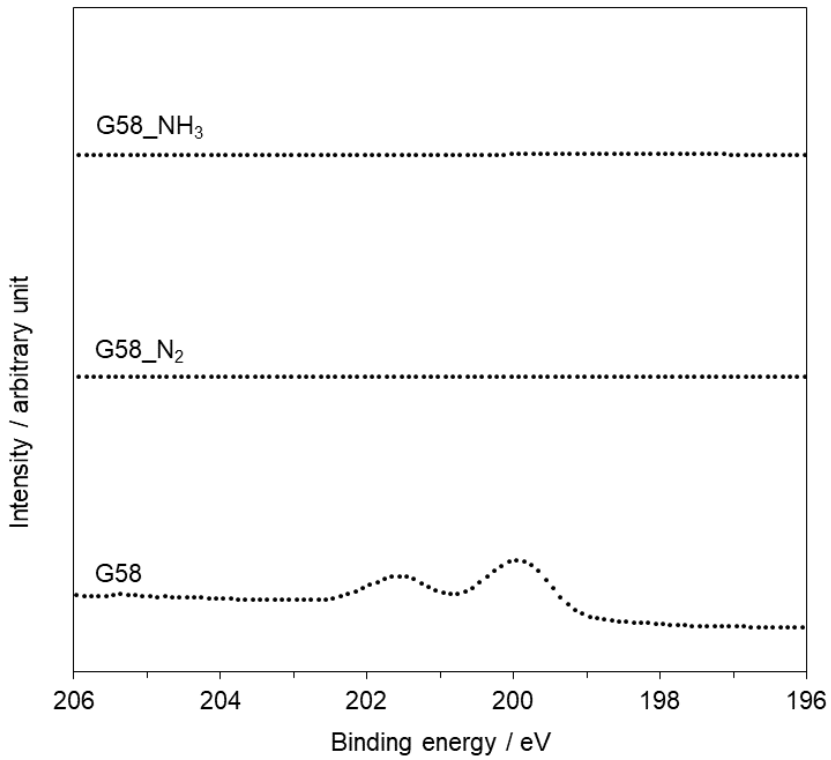

Fig. S6 The Cl 2p XPS spectra of G58 and its corresponding carbons.

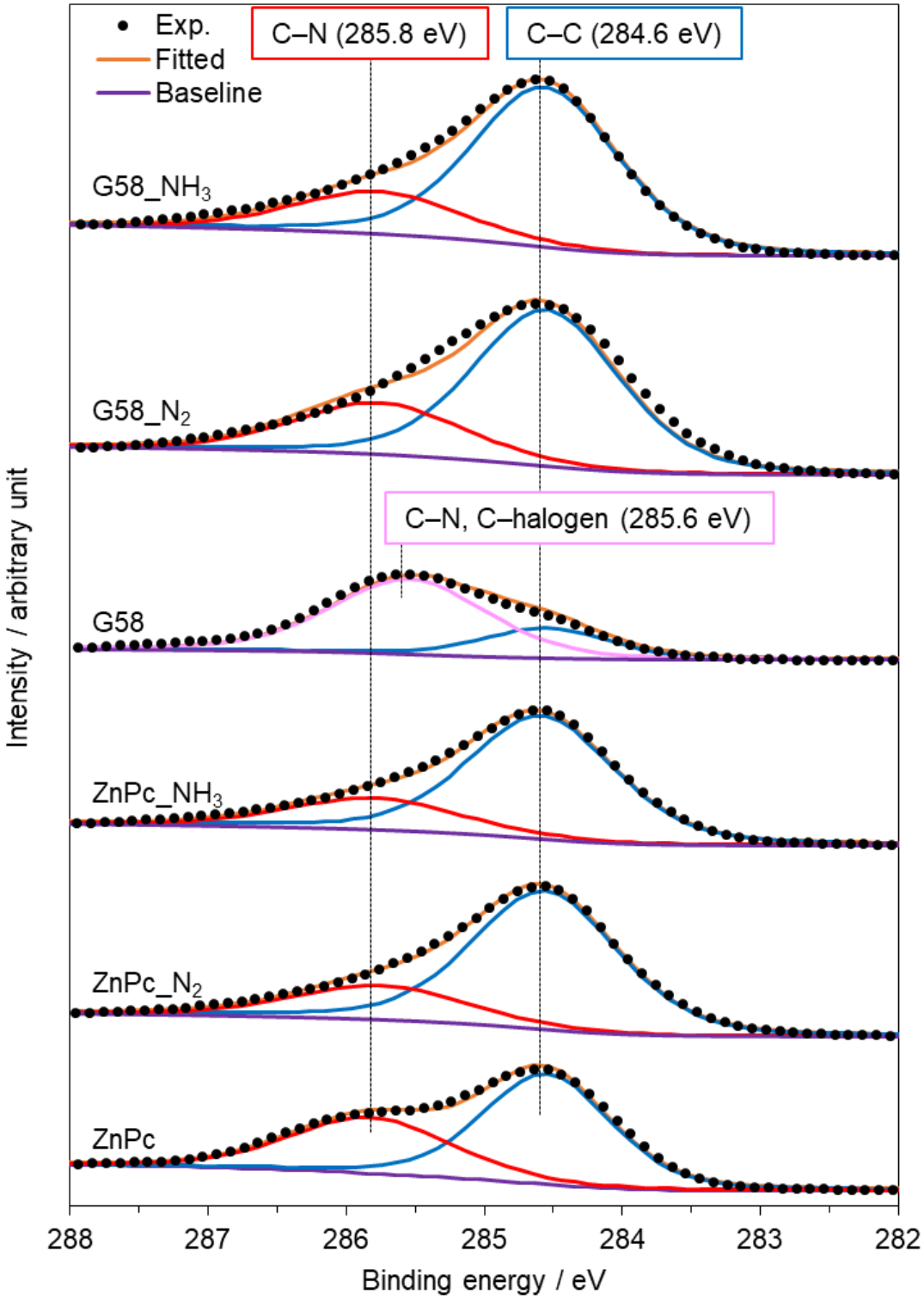

Fig. S7 The C 1s XPS spectra of ZnPc and G58 and their corresponding carbons.

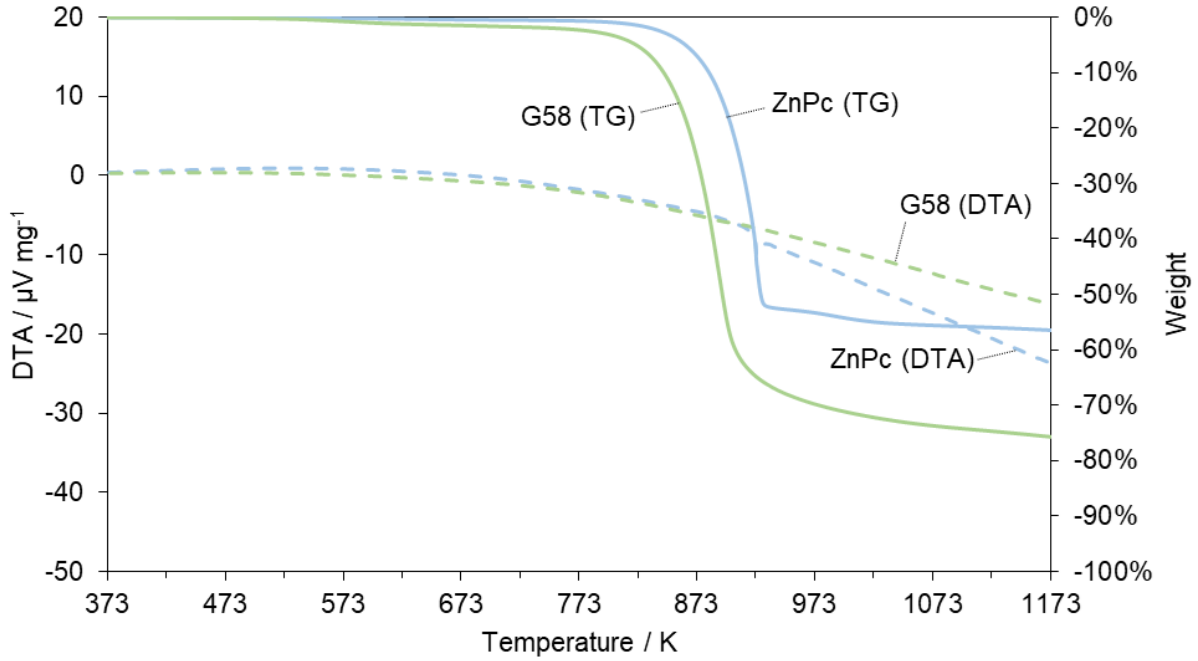

Fig. S8 TG-DTA data of ZnPc and G58 monitored under N_2 flow (heating rate: 10 K min^{-1}).

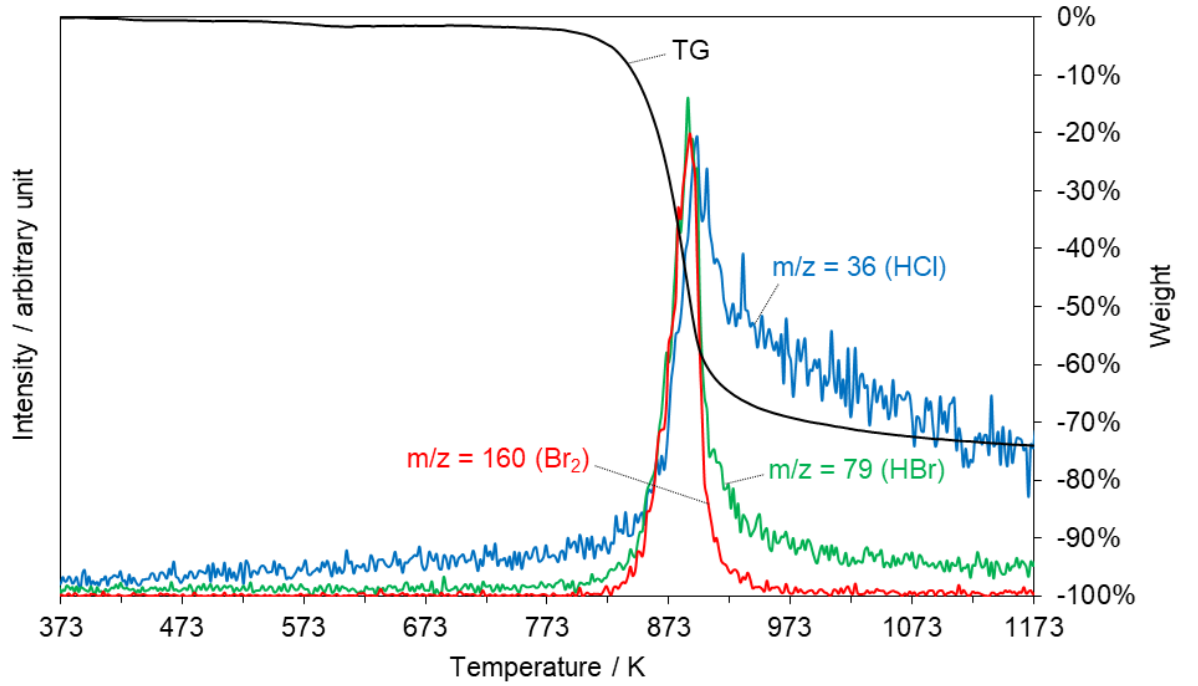

Fig. S9 TG-DTA/EI-MS data of G58 monitored under He flow (heating rate: 10 K min^{-1}). The profiles for the main halogen-containing components (HCl, HBr, and Br_2) are presented.

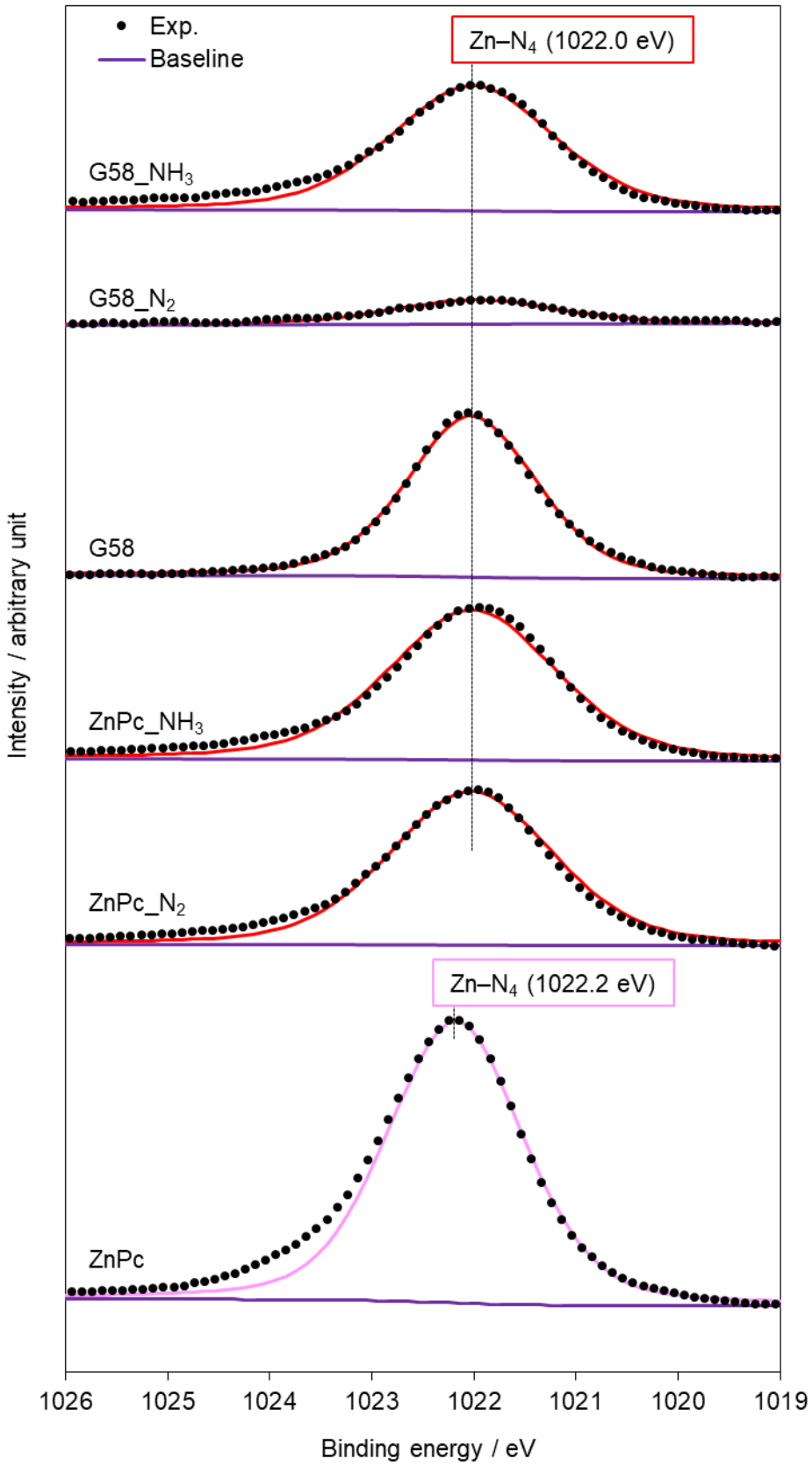

Fig. S10 The Zn $2p_{3/2}$ XPS spectra of ZnPc and G58 and their corresponding carbons.

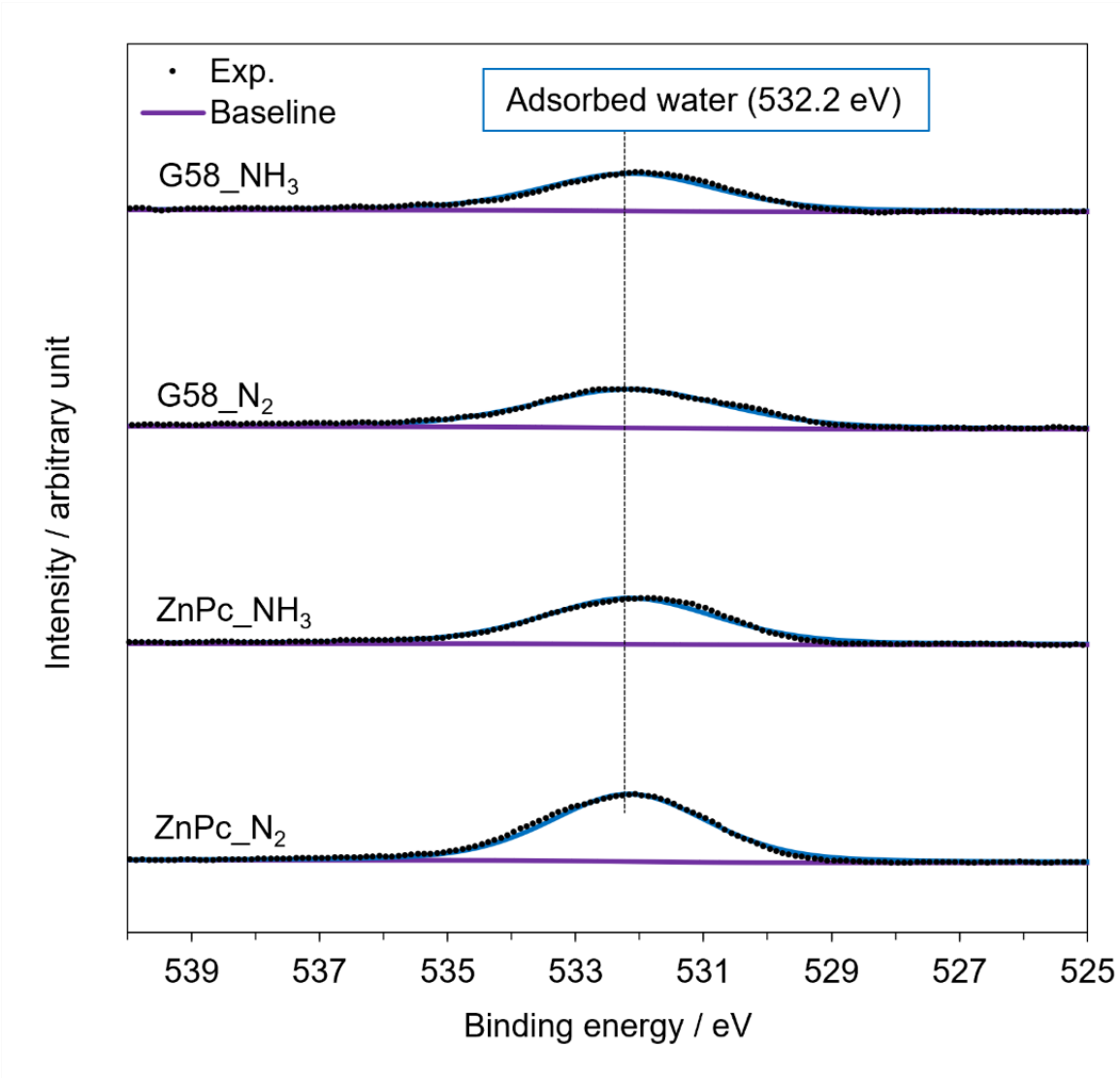

Fig. S11 The O 1s XPS spectra of the carbons.

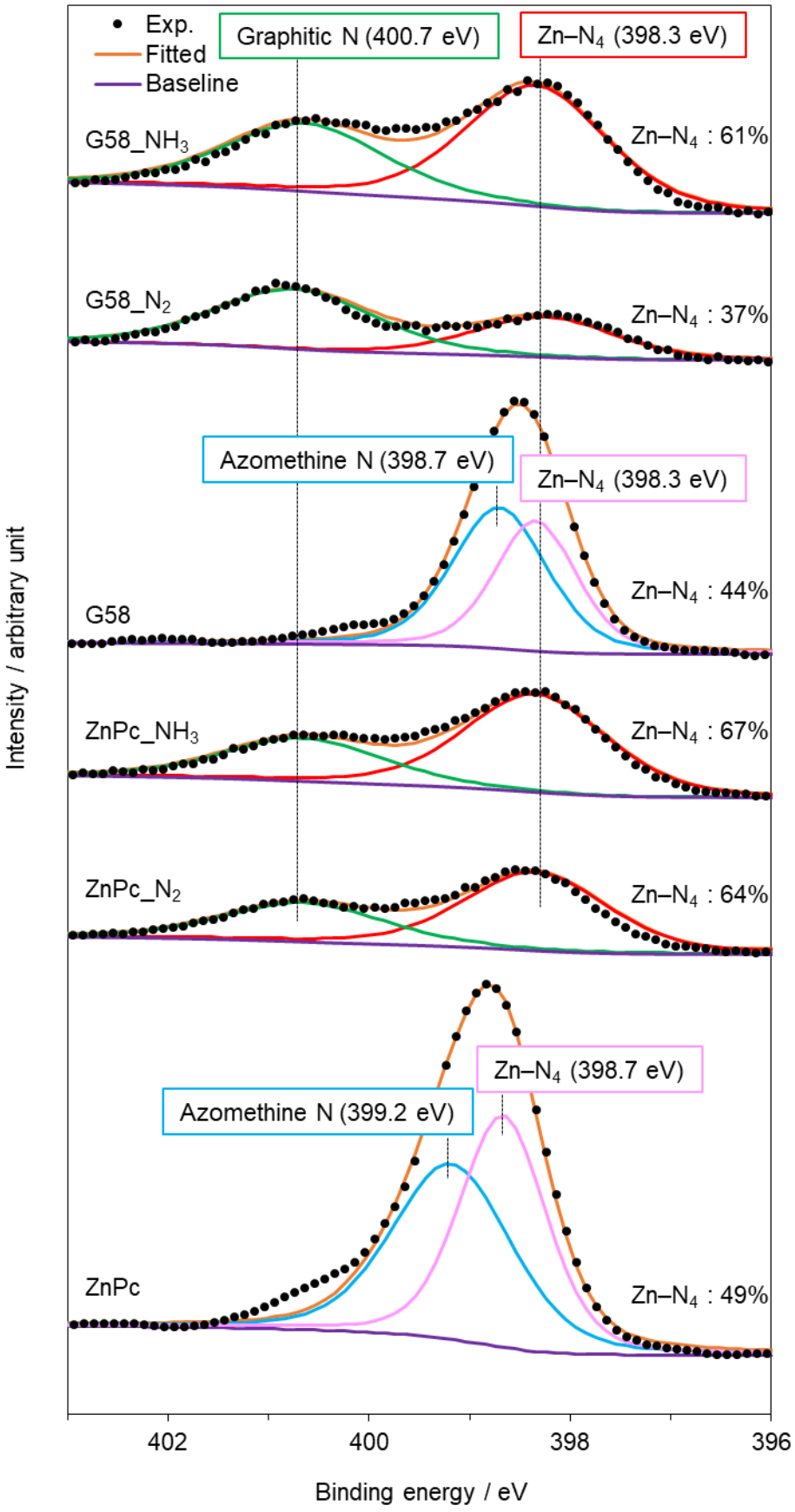

Fig. S12 The N 1s XPS spectra of ZnPc and G58 and their corresponding carbons.

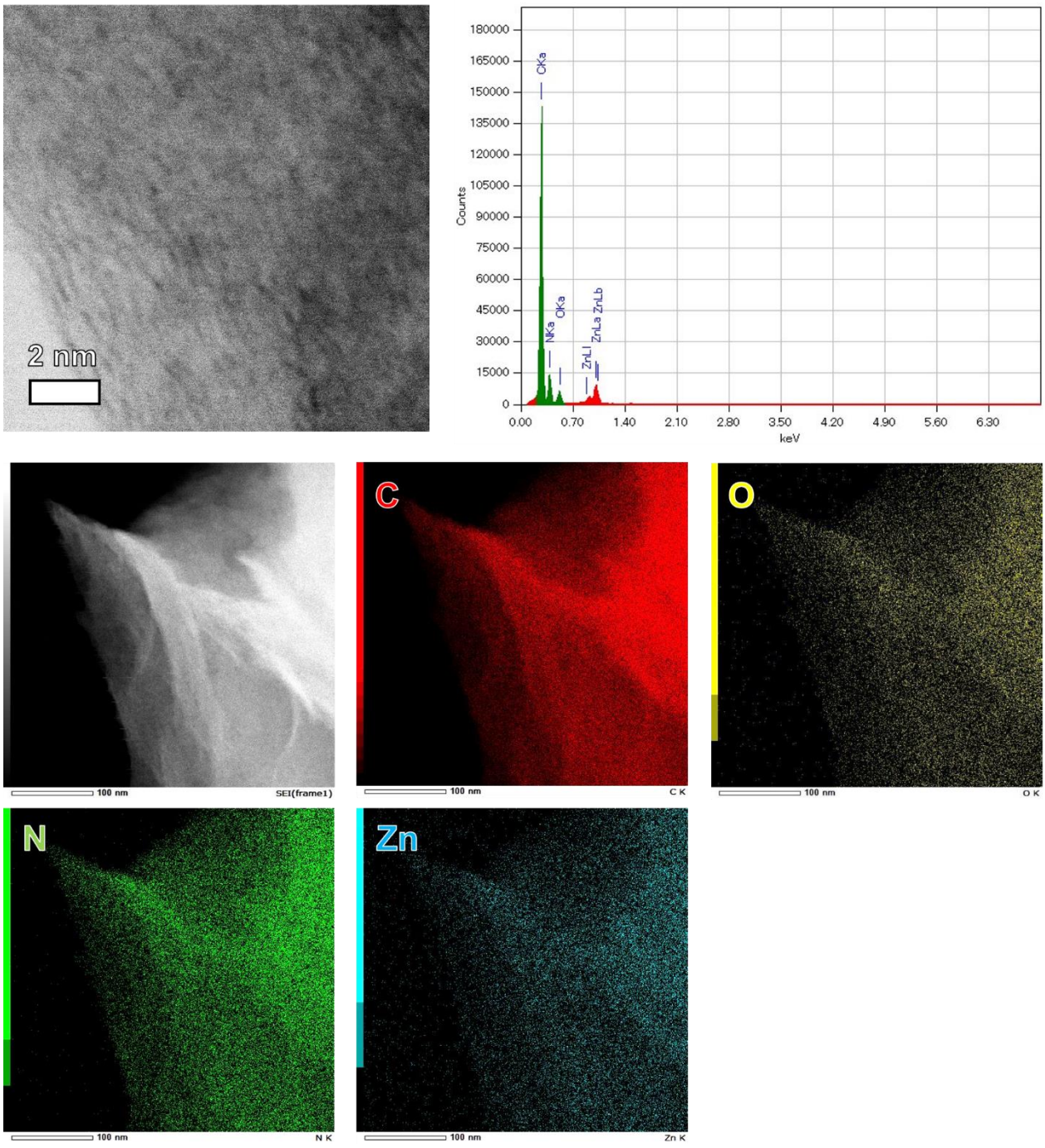

Fig. S13 STEM image, EDS mapping results and EDS spectrum of ZnPc_NH_3.

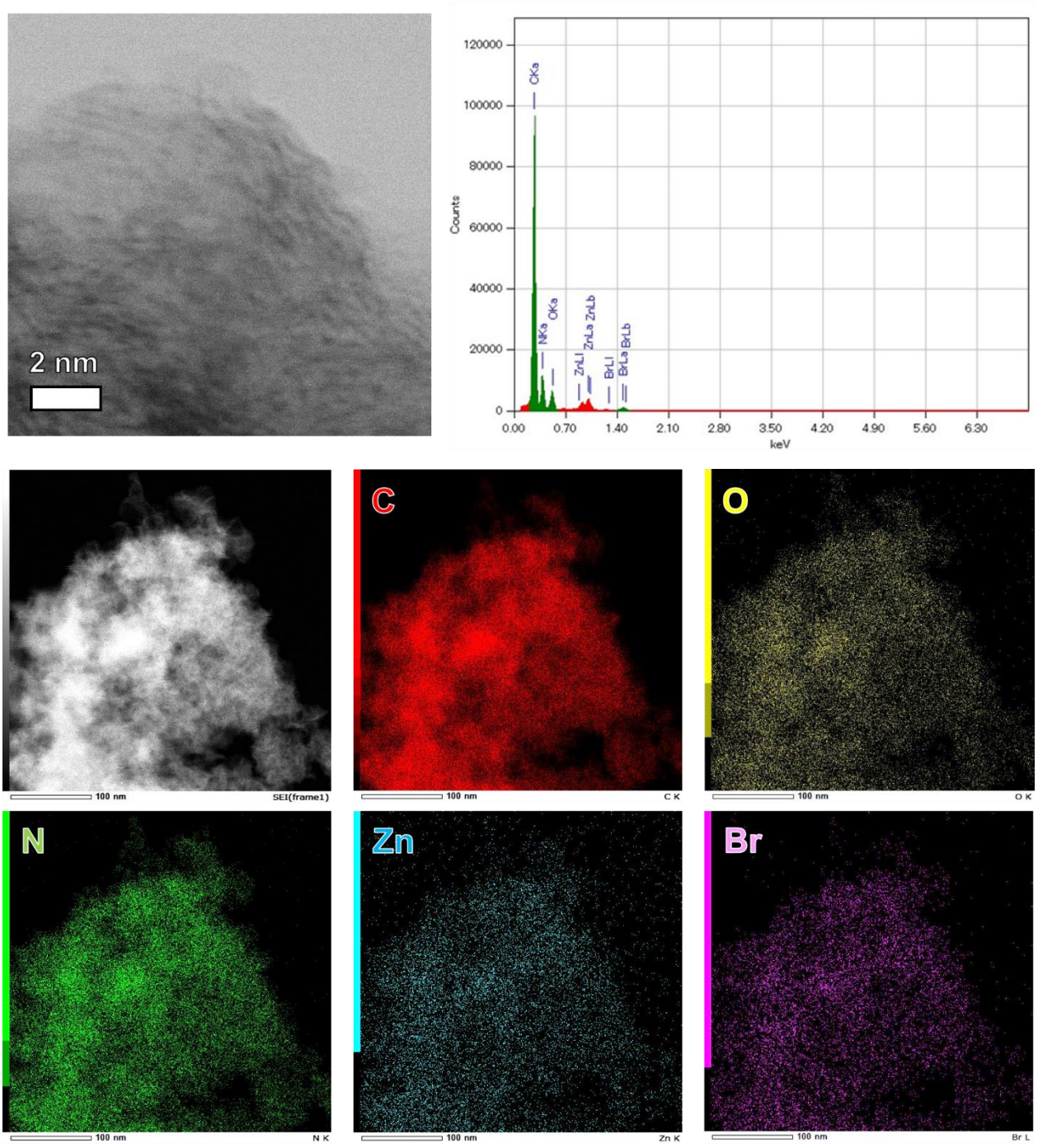

Fig. S14 STEM image, EDS mapping results and EDS spectrum of G58_NH_3.

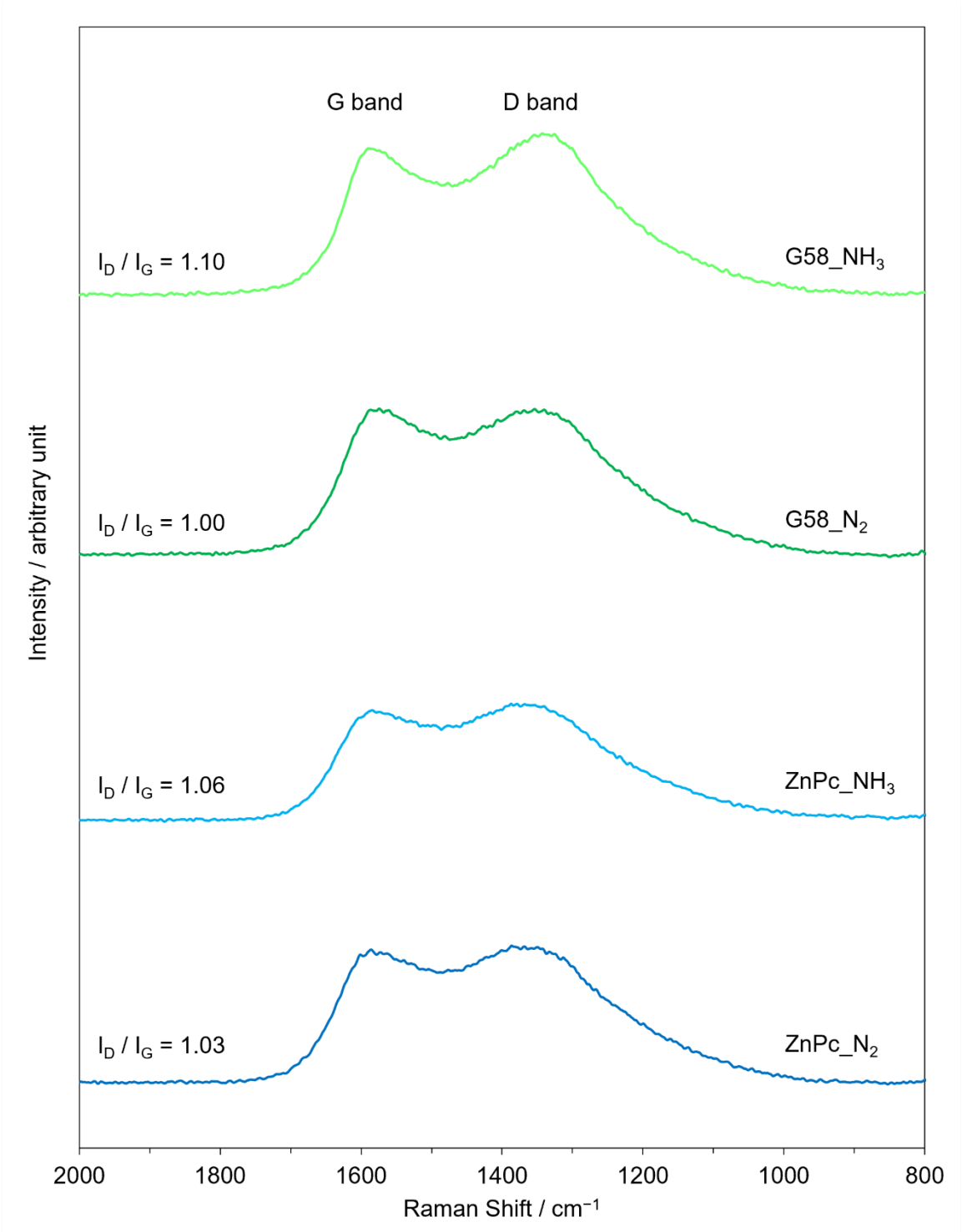

Fig. S15 Raman spectra of the carbons.

References

[1] R. Jiang, X. Chen, W. Liu, T. Wang, D. Qi, Q. Zhi, W. Liu, W. Li, K. Wang and J. Jiang, *ACS Appl. Energy Mater.*, 2021, **4**, 2481–2488.

[2] S. Yang, X. Xue, X. Liu, W. Liu, J. Bao, Y. Huang, H. Su, S. Yuan and H. Li, *ACS Appl. Mater. Interfaces*, 2019, **11**, 39263–39273.

[3] Y. Shiraishi, K. Kinoshita, K. Sakamoto, K. Yoshida, W. Hiramatsu, S. Ichikawa, S. Tanaka and T. Hirai, *Chem. Commun.*, 2024, **60**, 10866–10869.

[4] M. Muhyuddin, D. Testa, R. Lorenzi, G. Maria Vanacore, F. Poli, F. Soavi, S. Specchi, W. Giurlani, M. Innocenti, L. Rosi and C. Santoro, *Electrochim. Acta*, 2022, **433**, 141254.

[5] J.-H. Bang, B.-H. Lee, Y.-C. Choi, H.-M. Lee and B.-J. Kim, *Int. J. Mol. Sci.*, 2022, **23**, 8537.

[6] R. S. Mikhail, S. Brunauer and E. E. Bodor, *J. Colloid Interface Sci.*, 1968, **26**, 45–53.

[7] L. Osmieri, A. H.A. Monteverde Videla, M. Armandi and S. Specchia, *Int. J. Hydrogen. Energy*, 2016, **41**, 22570–22588.

[8] Q. Ma, G. Long, X. Tang, X. Li, X. Wang, C. You, W. Fan and Q. Wang, *Molecules*, 2023, **28**, 4257.

[9] J. Luo, K. Wang, X. Hua, W. Wang, J. Li, S. Zhang and S. Chen, *Small*, 2019, **15**, 1805325.

[10] J. Li, S. Chen, N. Yang, M. Deng, S. Ibraheem, J. Deng, J. Li, L. Li and Z. Wei, *Angew. Chem. Int. Ed.*, 2019, **58**, 7035–7039.

[11] T. Butburee, J. Ponchai, P. Khemthong, P. Mano, P. Chakthranont, S. Youngjan, J. Phanthasri, S. Namuangruk, K. Faungnawakij, X. Wang, Y. Chen and L. Zhang, *ACS Appl. Mater. Interfaces.*, 2024, **16**, 10227–10237.

[12] P. Song, M. Luo, X. Liu, W. Xing, W. Xu, Z. Jiang and L. Gu, *Adv. Funct. Mater.*, 2017, **27**, 1700802.